The Astrophysical Journal, 556:556–561, 2001 August 1

GRB 000418: A HIDDEN JET REVEALED

E. Berger,[1] A. Diercks,[1] D. A. Frail,[2] S. R. Kulkarni,[1] J. S. Bloom,[1] R. Sari,[3] J. Halpern,[4] N. Mirabal,[4] G. B. Taylor,[3] K. Hurley,[5] G. Pooley,[6] K. M. Becker,[7] R. M. Wagner,[8] D. M. Terndrup,[8] T. Statler,[9] D. R. Wik,[9] E. Mazets,[10] and T. Cline[11]

Received 2001 February 15; accepted 2001 April 5

ABSTRACT

We report on optical, near-infrared, and centimeter radio observations of GRB 000418 that allow us to follow the evolution of the afterglow from 2 to 200 days after the γ-ray burst (GRB). In modeling these broadband data, we find that an isotropic explosion in a constant-density medium is unable to simultaneously fit both the radio and optical data. However, a jetlike outflow into either a constant density or wind-stratified medium with an opening angle of 10°–20° provides a good description of the data. The evidence in favor of a jet interpretation is based on the behavior of the radio light curves, since the expected jet break is masked at optical wavelengths by the light of the host galaxy. We also find evidence for extinction, presumably arising from within the host galaxy, with $A_V^{\rm host} = 0.4$ mag, as well as host flux densities of $F_R = 1.1$ μJy and $F_K = 1.7$ μJy. These values supersede previous work on this burst as a result of the availability of a broadband data set allowing a global fitting approach. A model in which the GRB explodes isotropically into a wind-stratified circumburst medium cannot be ruled out by these data. However, in examining a sample of other bursts (e.g., GRB 990510, GRB 000301C), we favor the jet interpretation for GRB 000418.

Subject headings: gamma rays: bursts — infrared: general — radio continuum: general

1. INTRODUCTION

GRB 000418 was detected on 2000 April 18 at 09:53:10 UT by the *Ulysses* and *NEAR* spacecraft and the Konus *Wind*, which are part of the Third Interplanetary Network (IPN). The event lasted ~ 30 s, and a reanalysis of the early *Ulysses* data (Hurley, Cline, & Mazets 2000) gives a fluence of 4.7×10^{-6} ergs cm^{-2} in the 25–100 keV band. A fit to the total photon spectrum from the Konus data in the energy range 15–1000 keV gives a fluence of 2×10^{-5} ergs cm^{-2}. Intersecting IPN annuli resulted in a 35 arcmin^2 error box, in which Klose et al. (2000b) identified a variable near-infrared (NIR) source. The early R-band light curve of this source was described by Mirabal et al. (2000) as having a power-law decay $t^{-0.84}$, typical for optical afterglows. The redshift for the host galaxy of $z \simeq 1.119$ was measured by Bloom et al. (2000) from an [O II] emission-line doublet. Assuming cosmological parameters of $\Omega_M = 0.3$, $\Lambda_0 = 0.7$, and $H_0 = 65$ km s^{-1} Mpc^{-1}, this redshift corresponds to a luminosity distance $d_L = 2.5 \times 10^{28}$ cm and gives an implied isotropic γ-ray energy release of $E_\gamma = 1.7 \times 10^{52}$ ergs.

Klose et al. (2000a) have recently summarized optical/NIR data observations of GRB 000418. In this paper, we present additional optical/NIR data and a complete set of radio observations between 1.4 and 22 GHz from 10 to 200 days after the burst. We use this broadband data set to fit several models, deriving the physical parameters of the system.

2. OBSERVATIONS

2.1. *Optical Observations*

In Table 1 we present deep optical photometry obtained at the Palomar, Keck,[12] and MDM Observatories covering 6 weeks following the γ-ray burst (GRB), as well as data from the extant literature.

All of the optical data were overscan-corrected, flat-fielded, and combined in the usual manner using IRAF (Tody 1993). Point spread function fitting photometry was performed using Dophot (Schechter, Mateo, & Saha 1993) relative to several local comparison stars measured by Henden (2000). Short exposures of the field in each band were used to transfer the photometry (Henden 2000) to several fainter stars in the field. Several of the Keck Echellette Spectrograph and Imager (ESI) measurements and the Palomar 200 inch (5 m) measurement were made in Gunn r and Gunn i, respectively, and were calibrated by transforming the local comparison stars to the Gunn system using standard transformations (Wade et al. 1979; Jørgensen 1994). We add an additional 5% uncertainty in quadrature with the statistical uncertainties to reflect the inherent imprecision in these transformations.

[1] Palomar Observatory, Mail Code 105-24, California Institute of Technology, Pasadena, CA 91125.
[2] National Radio Astronomy Observatory, P.O. Box O, Socorro, NM 87801.
[3] Theoretical Astrophysics, Mail Code 103-33, California Institute of Technology, 1201 East California Boulevard, Pasadena, CA 91125.
[4] Department of Astronomy, Columbia University, 550 West 120th Street, New York, NY 10027.
[5] Space Sciences Laboratory, University of California, Berkeley, CA 94720-7450.
[6] Mullard Radio Astronomy Observatory, Cavendish Laboratory, Madingley Road, Cambridge CB3 0HE, UK.
[7] Department of Physics, Oberlin College, Oberlin, OH 44074.
[8] Department of Astronomy, Ohio State University, 140 West 18th Avenue, Columbus, OH 43210-1173.
[9] Department of Physics and Astronomy, Clippinger Research Labs, Ohio University, 251B, Athens, OH 45701.
[10] Ioffe Physico-Technical Institute, 26 Polytekhnicheskaya, St. Petersburg 194021, Russia.
[11] NASA Goddard Space Flight Center, Code 661, Greenbelt, MD 20771.

[12] The W. M. Keck Observatory is operated by the California Association for Research in Astronomy, a scientific partnership among the California Institute of Technology, the University of California, and the National Aeronautics and Space Administration.

TABLE 1

OPTICAL/NIR OBSERVATIONS OF GRB 000418

UT Date (2000)	Instr.[a]	Band	Mag.[b]	Error	Ref.
Apr 20.89	TNG 3.5 m	*R*	21.54	0.04	1
Apr 20.90	CA 3.5 m	*K'*	17.49	0.5	1
Apr 20.93	CA 1.2 m	*K'*	17.89	0.2	1
Apr 21.15	MDM 2.4 m	*R*	21.66	0.12	2
Apr 21.86	LO 1.5 m	*R*	21.92	0.14	1
Apr 26.316	USNO 1.3 m	*R*	22.65	0.20	1, 3
Apr 27.26	MDM	*R*	22.77	0.23	2
Apr 28.170	P200	*R*	22.97	0.06	2
Apr 28.3	MDM	*R*	22.86	0.09	2
Apr 28.413	Keck/ESI	*R*	23.05	0.05	2
Apr 29.26	MDM	*R*	22.95	0.11	2
May 2.274	Keck/ESI	Gunn *i*	23.38	0.05	2
May 2.28	MDM	*R*	23.19	0.12	2
May 2.285	Keck/ESI	*B*	24.31	0.08	2
May 2.31	USNO 1.3 m	*R*	23.11	0.130	1
May 3.26	USNO 1.3 m	*R*	23.41	0.160	1
May 4.44	UKIRT 3.8 m	*K*	20.49	0.40	1
May 6.42	Keck/LRIS	*R*	23.48	0.10	4
May 8.89	TNG	*R*	23.30	0.05	1
May 8.92	TNG	*V*	23.92	0.07	1
May 9.82	USNO 1.0 m	*R*	23.37	0.21	1
May 23.93	TNG	*R*	23.37	0.10	1
May 29.228.....	P200	*R*	23.66	0.15	2
Jun 2.88	CA 3.5 m	*R*	23.32	0.08	1
Jun 2.91	TNG	*R*	23.57	0.05	1

[a] CA 3.5 m = Calar Alto 3.5 m telescope, USNO 1.3 m = U.S. Naval Observatory Flagstaff Station 1.3 m telescope, ESI = W. M. Keck Observatory Echellette Spectrograph and Imager, and LRIS = W. M. Keck Observatory Low Resolution Imaging Spectrograph.

[b] Optical photometry is on the Kron-Cousins and Gunn systems and referred to that of Henden 2000. Data are corrected for Galactic extinction corresponding to $E(B-V) = 0.032$ derived from the maps of Schlegel et al. 1998.

REFERENCES.—(1) Klose et al. 2000a; (2) this work; (3) Henden et al. 2000; (4) Metzger & Fruchter 2000.

The K_s-band image of the field was obtained on the Keck I Telescope on Mauna Kea, Hawaii, with the Near Infrared Camera. We obtained a total of 63 exposures of 1 minute duration, which we reduced and combined with the IRAF DIMSUM package. There was significant cloud and cirrus cover, so the night was not photometric.

The *Hubble Space Telescope* STIS clear image was obtained on 2000 June 4 UT as part of the Target of Opportunity program 8189 (principal investigator, A. Fruchter) and made public on 2000 September 2 UT. Five images of 500 s each were obtained, which we combined using the IRAF DITHER task. The final plate scale is 25 mas pixel^{-1}.

We corrected all optical measurements in Table 1 for a Galactic foreground reddening of $E(B-V) = 0.032$ (Schlegel, Finkbeiner, & Davis 1998) at the position of the burst $(l, b) = (261\overset{\circ}{.}16, 80\overset{\circ}{.}78)$ before converting to flux units (Fukugita, Shimasaku, & Ichikawa 1995; Bessell & Brett 1988) assuming $R_V = 3.1$.

2.2. *Radio Observations*

Radio observations were undertaken at a frequency of 15 GHz with the Ryle Telescope. All other frequencies were observed with either the NRAO[13] Very Large Array (VLA) or the Very Long Baseline Array (VLBA). A log of these observations can be found in Table 2. The data acquisition and calibration for the Ryle and the VLA were straightforward (see Frail et al. 2000a for details).

[13] NRAO is a facility of the National Science Foundation operated under cooperative agreement by Associated Universities, Inc. NRAO operates the VLA and the VLBA.

TABLE 2

RADIO OBSERVATIONS OF GRB 000418

Epoch (2000 UT)	Telescope	ν_0 (GHz)	$S \pm \sigma$ (μJy)
Apr 28.75	Ryle	15.0	550 ± 600
Apr 29.07	VLA	8.46	856 ± 33
Apr 30.07	VLA	8.46	795 ± 37
Apr 30.73	Ryle	15.0	1350 ± 480
May 1.06	VLA	4.86	110 ± 52
May 1.06	VLA	8.46	684 ± 48
May 2.93	Ryle	15.0	850 ± 300
May 3.04	VLA	4.86	1120 ± 52
May 3.04	VLA	8.46	1240 ± 46
May 3.04	VLA	22.46	1100 ± 150
May 4.97	VLA	1.43	210 ± 180
May 4.97	VLA	4.86	710 ± 47
May 4.97	VLA	8.46	1020 ± 53
May 4.97	VLA	22.46	860 ± 141
May 7.18	VLBA	8.35	625 ± 60
May 9.25	VLA	8.46	926 ± 53
May 16.13.....	VLA	8.46	963 ± 34
May 18.24.....	VLA	4.86	567 ± 50
May 18.24.....	VLA	8.46	660 ± 50
May 18.24.....	VLA	22.46	610 ± 114
May 22.21.....	VLA	8.46	643 ± 38
May 26.92.....	VLA	4.86	1105 ± 51
May 26.92.....	VLA	8.46	341 ± 50
Jun 1.14	VLA	8.46	556 ± 43
Jun 1.14	VLA	22.46	710 ± 16
Jun 3.04	VLA	8.46	517 ± 34
Jun 7.01	VLA	8.46	238 ± 38
Jun 11.93.....	VLA	8.46	230 ± 33
Jun 15.13.....	VLA	8.46	325 ± 30
Jun 20.10.....	VLA	8.46	316 ± 30
Jun 23.19.....	VLA	8.46	306 ± 29
Jun 27.08.....	VLA	8.46	296 ± 22
Jul 02.98.....	VLA	8.46	274 ± 22
Jul 10.04.....	VLA	8.46	178 ± 24
Jul 22.81.....	VLA	8.46	152 ± 23
Jul 22.81.....	VLA	4.86	192 ± 25
Jul 28.50.....	VLA	8.46	168 ± 22
Jul 28.50.....	VLA	4.86	191 ± 25
Aug 17.74	VLA	8.46	119 ± 25
Aug 17.74	VLA	4.86	235 ± 31
Aug 21.65	VLA	4.86	142 ± 35
Aug 21.65	VLA	8.46	87 ± 31
Aug 25.78	VLA	4.86	238 ± 34
Aug 25.78	VLA	8.46	166 ± 27
Aug 27.89	VLA	8.46	100 ± 25
Sep 10.73.....	VLA	8.46	148 ± 25
Sep 18.68.....	VLA	8.46	55 ± 20
Sep 26.62.....	VLA	8.46	85 ± 22
Nov 06.55	VLA	8.46	94 ± 14

NOTE.—The columns are (left to right), (1) UT date of the start of each observation, (2) telescope name, (3) observing frequency, and (4) peak flux density at the best-fit position of the radio transient, with the error given as the rms noise on the image.

The single VLBA observation was carried out at 8.35 GHz with a total bandwidth of 64 MHz in a single polarization, using 2 bit sampling for additional sensitivity. The nearby ($<11.^{\circ}3$) calibrator J1224+2122 was observed every 3 minutes for delay, rate, and phase calibration. Amplitude calibration was obtained by measurements of the system temperature in the standard way. The coordinates for GRB 000418 derived from the VLBA detection are (epoch J2000) $\alpha = 12^{h}25^{m}19^{s}.2840$ ($\pm 0^{s}.015$), $\delta = +20^{\circ}06'11''.141$ ($\pm 0''.001$).

3. THE OPTICAL LIGHT CURVE AND HOST GALAXY

In Figure 1 we display the *R*- and *K*-band light curves constructed from measurements in Table 1. The pronounced flattening of the *R*-band light curve at late times is reasonably attributed to the optical afterglow fading below the brightness of the underlying host galaxy. A noise-weighted least-squares fit was made to the data of the form $f_R = f_o t_o^{\alpha} + f_{\rm host}$, for which we derive $f_o = 23.4 \pm 2.1$ μJy, $\alpha_o = -1.41 \pm 0.08$, and $f_{\rm host} = 1.08 \pm 0.06$ μJy with a reduced $\chi_r^2 = 0.94$. Our inferred *R*-band magnitude for the host galaxy, $R_{\rm host} = 23.66 \pm 0.06$, is nearly identical to that obtained from a similar analysis by Klose et al. (2000a). In order to estimate the effect of the host in other optical bands, we scaled $R_{\rm host}$ for GRB 000418 to a spectrum of the host galaxy of GRB 980703 ($z = 0.966$; Bloom et al. 1998), whose magnitude was measured in seven broadband colors (*B*, *V*, *R*, *I*, *J*, *H*, and *K*). Our results indicate that 50%–100% of the flux in some bands is due to the host galaxy after the first 10 days. Therefore, for the afterglow modeling in § 5 we chose not to include the late-time measurements of GRB 000418 in the *B*, *V*, and Gunn *i* bands.

4. THE RADIO LIGHT CURVES

In Figure 1 we display the radio light curves at 4.86, 8.46, 15, and 22 GHz. To first order all four frequencies show a maximum near 1 mJy on a timescale of 10–20 days. There is no discernible rising trend at any frequency. This is most clear at 8.46 GHz, where the light curve undergoes a steady decline beginning 10 days after the burst, fading from 1 to 0.1 mJy over a 6 month period. The temporal slope of the 8.46 GHz light curve after the first 2 months, $\alpha_{\rm rad} = -1.37 \pm 0.10$ ($\chi_r^2 = 1.4$), is similar to the optical *R*-band curve $\alpha_{\rm opt} = -1.41 \pm 0.08$.

Superposed on this secular decrease, there exist point-to-point variations on the order of 50%, especially in the early measurements. We attribute these variations to interstellar scintillation (ISS; Goodman 1997; Walker 1998). The method by which we estimate the magnitude of the intensity fluctuations induced by ISS as a function of frequency and time is described in full in Berger et al. (2000). Briefly, we estimate the magnitude of scattering with the model of

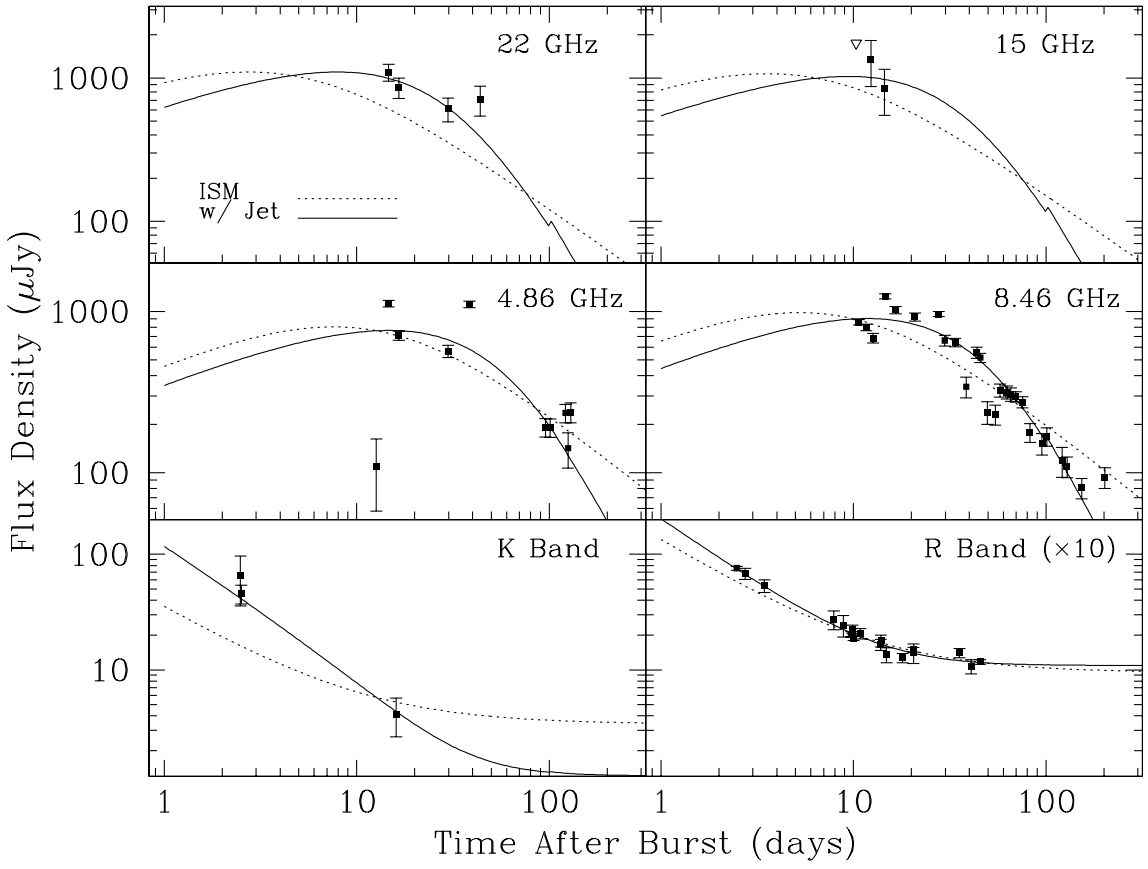

FIG. 1.—Radio and optical light curves for GRB 000418. The observing frequency (or band) is shown in the upper right corner of each panel. Optical magnitudes were first corrected for Galactic foreground reddening before converting to flux units. For display purposes, the *R*-band flux densities have been increased by a factor of 10. The 8.46 GHz measurements on August 25 and September 18 are three-epoch averages taken over a period of 7 and 15 days, respectively. The dotted and solid lines are light curves assuming an isotropic explosion in a constant-density medium (ISM), and collimated ejecta with opening angle θ_j (ISM + jet), respectively. They were derived from a global fit to the entire broadband data set.

Taylor & Cordes (1993) and use this to calculate the transition frequency ν_0 between weak and strong scattering using the prescription of Walker (1998). The normalizations used in Goodman (1997) give slightly larger values of ν_0.

In the direction toward GRB 000418, we derive $\nu_0 \simeq 3.6$ GHz, and therefore most of our measurements were taken in the weak ISS regime. In this case the modulation scales as $\nu^{-17/12}$, with a maximum of 65% expected at 4.86 GHz and 30% at 8.46 GHz. At 15 and 22 GHz, we estimate that the ISS-induced fluctuations are only a fraction of the instrumental noise. The expansion of the fireball will eventually quench ISS when the angular size of the fireball exceeds the angular size of the first Fresnel zone at the distance of the scattering screen. The fireball size, and hence the quenching timescale, is model dependent, and we use the derived total energy and density from the global fits (see § 5 below) to estimate this time for each model. For example, in a simple spherical fireball, this occurs after 15 days at 4.86 GHz and after 10 days at 8.46 GHz, and thereafter the modulation indices decline as $t^{-35/48}$. We note that the observed fluctuations at 4.86 and 8.46 GHz conform to the predicted level of ISS, but that the measurements at 8.46 GHz from around 50 days after the burst deviate by a factor of 3 from the predicted ISS level.

In addition, we use the scintillation pattern to estimate the true χ^2_r for each model by adding in quadrature to the instrumental noise an additional ISS-induced uncertainty, $\sigma_{\rm ISS} = m_p F_{\nu,\rm model}$, where m_p and $F_{\nu,\rm model}$ are the modulation index and model flux density at frequency ν, respectively (Berger et al. 2000).

5. GLOBAL MODEL FITS

The optical and radio data presented here have allowed us to track the evolution of the GRB 000418 afterglow from 2 to 200 days after the burst. With careful modeling of the light curves, it should be possible to infer the physical parameters of the blast wave and thereby gain some insight into the nature of GRB progenitors. In particular, the hydrodynamic evolution of the shock is governed by the energy of the explosion, the geometry of the expanding ejecta shock, and the type of environment into which the GRB explodes (Sari, Piran, & Narayan 1998; Wijers & Galama 1999; Chevalier & Li 1999; Panaitescu & Kumar 2000). We will consider four basic models: a spherical explosion or collimated ejecta (i.e., jets) in both a constant-density medium and in a windblown medium.

The starting point for any afterglow interpretation is the cosmological fireball model (e.g., Mészáros & Rees 1997; Waxman 1997). A point explosion of energy E_0 expands relativistically into the surrounding medium (with density $\rho \propto r^{-s}$, where $s = 0$ for a constant-density interstellar medium and $s = 2$ for a wind), and the shock produced as a result of this interaction is a site for particle acceleration. The distribution of electrons is assumed to be a power law of index p, and the fraction of the shock energy available for the electrons and magnetic field is ϵ_e and ϵ_B, respectively. The values of these three quantities (p, ϵ_e, and ϵ_B) are determined by the physics of the shock and the process of particle acceleration and, in the absence of detailed understanding, are taken to be constant with time.

The instantaneous broadband synchrotron spectrum can be uniquely specified by the three characteristic frequencies ν_a, ν_m, and ν_c (i.e., synchrotron self-absorption, synchrotron peak, and cooling), the peak flux density f_m, and p. For this work we adopt the smooth spectral shape as given by Granot, Piran, & Sari (1999a, 1999b) rather than the piecewise, broken power-law spectrum used by other authors (e.g., Wijers & Galama 1999). The evolution of the spectrum (and thus the time dependence of ν_a, ν_m, ν_c, and f_m) is governed by the geometry of the explosion (spherical or collimated into a jetlike outflow) and the properties of the external environment (constant-density or a radial density profile). Our approach is to adopt a model (sphere, wind, jet, etc.) and solve for the above spectral parameters using the entire optical and radio data set. The advantages and details of global model fitting are discussed in Berger et al. (2000).

The simplest model is a spherically symmetric explosion in a constant-density medium (the ISM model; Sari et al. 1998). The total χ^2_r for this model (see Table 3) gives a highly unsatisfactory fit to the data. On close inspection (Fig. 1), we find that the model systematically underpredicts the optical flux. Adding extinction from the host galaxy only makes this worse. The fundamental difficulty with the ISM model is that it predicts f_m = constant, independent of frequency. In this case, since it is the radio data that are responsible for defining the peak of the spectrum, it results in a value of f_m that is too low at higher frequencies.

To obtain better fits to the joint optical and radio data sets, we look to models for which f_m is time dependent. One such model is a collimated outflow into a medium with uniform density (the ISM + jet model; Rhoads 1997, 1999; Sari, Piran, & Halpern 1999). The clearest observational signature of a jet is an achromatic break in the light curves at t_j (see, e.g., Harrison et al. 1999). At radio wavelengths (i.e., below ν_m) at t_j, we expect a transition from a rising $t^{1/2}$ light curve to a shallow decay of $t^{-1/3}$, while at optical wavelengths the decay is expected to steepen to t^{-p}. These decay indices refer to the asymptotic values.

TABLE 3

MODEL PARAMETERS FOR GRB 000418

Parameters	ISM	ISM + Jet	Wind	Wind + Jet
ν_a (Hz)	4.1×10^9	1.7×10^9	30×10^9	3.7×10^9
ν_m (Hz)	2.3×10^{11}	1.8×10^{10}	5.8×10^{11}	1.1×10^{11}
ν_c (Hz)	2×10^{15}	10^{14}	1.8×10^{13}	5×10^{12}
f_m (mJy)	2.5	3.4	10.4	3.7
p	2.3	2.4	2.2	2.5
t_j (days)	...	25.7	...	14.6
$A_V^{\rm host}$	0.0	0.4	0.3	0.2
χ^2/dof	326/54	165/53	184/53	127/53
E_{52}	11	10	4	1.6
n_0 or A^*	0.01	0.02	0.14	0.07
ϵ_B	0.05	0.06	0.04	0.70
ϵ_e	0.03	0.10	0.07	0.14

NOTE.—For the ISM and wind models, ν_a, ν_m, ν_c, and f_m are the self-absorption, synchrotron peak, cooling frequencies, and the peak flux density, respectively, on day 1. For the ISM + jet and wind + jet models, these values are referenced instead to the jet break time t_j. The parameter p is the electron power-law index and A_V is the V-band extinction in the rest frame of the host galaxy ($z = 1.118$), assuming an LMC-like extinction curve. The resulting values of χ^2 include an estimated contribution of interstellar scattering (ISS) and the increased error in subtracting off a host galaxy flux from each of the optical points. The model parameters are the total isotropic energy E_{52} in units of 10^{52} ergs, the ambient density n_0 in cm^{-3} or, in the case of the two wind models, the parameter A^* as defined by Chevalier & Li 1999. The parameters ϵ_e and ϵ_B are the fraction of the shock energy in the electrons and the magnetic field, respectively. The true uncertainties in the derived parameters are difficult to quantify because of covariance, but we estimate that they range from 10% to 20%.

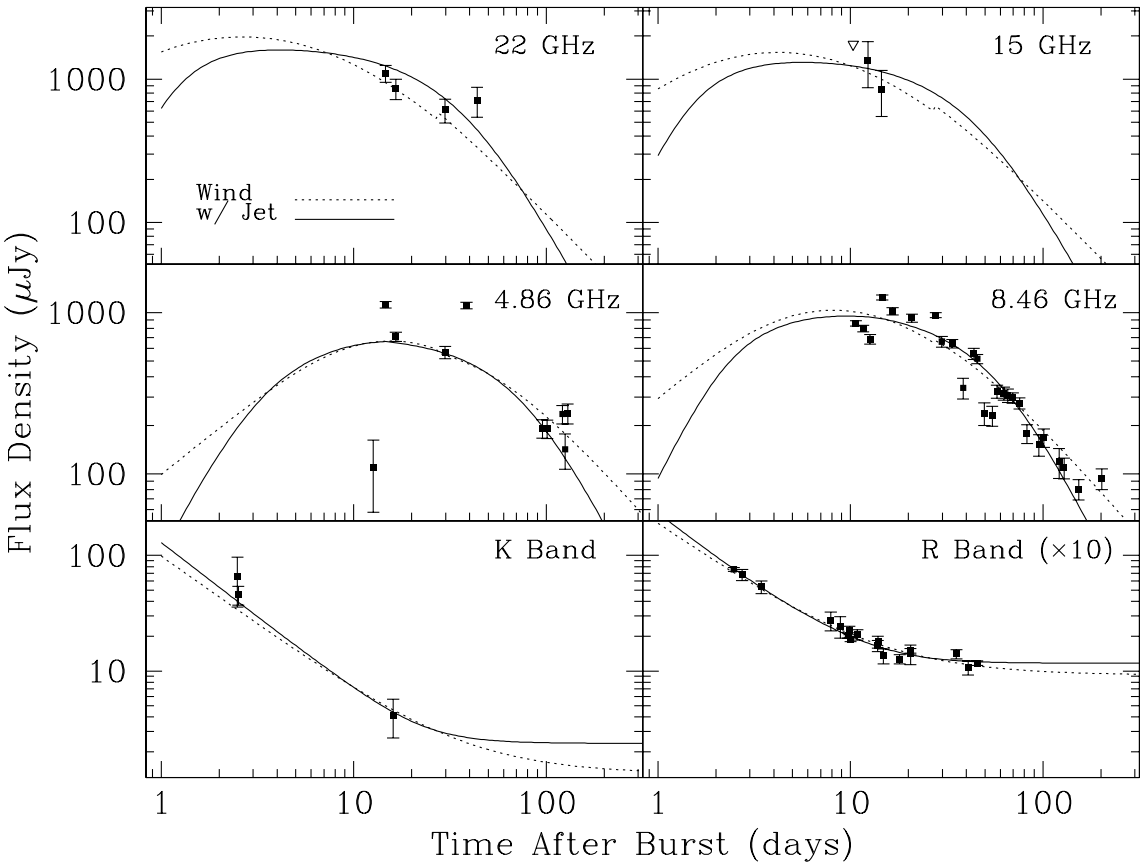

FIG. 2.—Similar to Fig. 1, but dotted and solid lines are light curves assuming an isotropic explosion in a windblown circumburst medium (wind) and collimated ejecta with opening angle θ_j (wind + jet), respectively.

Detecting a jet transition at optical wavelengths may be difficult if it occurs on timescales of a week or more. In these cases, the afterglow is weak and the light from the host galaxy may start to dominate the light curve (e.g., Halpern et al. 2000). In such instances radio observations may be required to clarify matters, since the radio flux is increasing prior to t_j and changes in the light-curve evolution due to the jet break are easily detected. Indeed, the jet in GRB 970508, which was very well observed in the radio, is not discernible in the optical data. In this case, Frail, Waxman, & Kulkarni (2000) found a wide-angle jet with an opening angle of 30° and $t_j \sim 30$ days (but see Chevalier & Li 2000).

An ISM + jet model with $t_j \approx 26$ days fits the data remarkably well (see Fig. 1). The strongest point in favor of this model is that it reproduces the broad maximum (~ 1 mJy) seen from 5 to 22 GHz. We expect such a plateau at t_j, since all light curves for $\nu_a < \nu \leq \nu_m$ reach their peak fluxes (with only a weak $\nu^{1/3}$ frequency dependence) before undergoing a slow decline. Most other models predict a strong frequency dependence in peak flux that is not seen in this case.

Knowing t_j and the density of the ambient medium n_0 from the model fit (Table 3), we can make a geometric correction to the total isotropic energy E_γ, as determined from either the observed γ-ray fluence or the total energy of the afterglow E_{52}, from the fit to the afterglow data (Sari et al. 1999; Livio & Waxman 2000). This approach gives values for the jet opening angle θ_j of between 10° and 20°, which for a two-sided jet reduces the GRB energy to $\sim 10^{51}$ ergs. The rapid lateral expansion of the jet also accelerates the transition to the nonrelativistic regime, resulting in a change in the evolution of the light curves. Since this occurs on a timescale of $t_{\rm NR} \sim t_j \theta_j^{-2} \sim 350$ days (Waxman, Kulkarni, & Frail 1998), we do not expect the nonrelativistic transition to be important for our data.

There is some freedom in our choice of ν_c. We know that a cooling break (i.e., $\Delta\alpha = -0.25$) is not apparent in the R-band light curve on timescales of 2–10 days, so we searched for solutions with ν_c above or below this frequency. We found that physically consistent solutions (i.e., with nonnegative host fluxes and $\epsilon_B < 1$) were only possible for values of ν_c below the optical band.

As part of the fitting process, we also solved for the host flux density in the i and K bands and for any local dust obscuration, assuming an LMC-like extinction law. This yields $f_{\rm host}(R) = 1.1$ μJy, $f_{\rm host}(K) = 1.7$ μJy, and $A_V^{\rm host} = 0.4$ (in the host galaxy rest frame). Klose et al. (2000b) argued for significant dust extinction with $A_V^{\rm host} = 0.96$. However, they likely overestimated $A_V^{\rm host}$, since they assumed a spherical fireball model and arbitrarily located ν_c above the optical band. Moreover, we find that there is some covariance between the values of $A_V^{\rm host}$ and p, so that only with a global fit, in which p is constrained by the radio data as well as the optical data, can we solve for $A_V^{\rm host}$ in a self-consistent manner.

In view of the claims linking GRBs with the collapse of massive stars (Galama et al. 1998; Bloom et al. 1999; Reichart 1999; Piro et al. 2000), we considered models of either spherical or jetlike explosions into a windblown circumburst medium (the wind model; Chevalier & Li 1999; Li & Chevalier 1999). The wind models (Fig. 2) fit the data as well as the ISM + jet model. In fact, the χ^2 is lowest for the

wind+jet model. However, in view of the uncertainties in estimating the contribution of ISS to the radio flux variations (see § 4), we do not consider these differences to be significant. The close match between the temporal slopes of the late-time 8.46 GHz light curve and the early R-band light curve (see § 4) is a point in favor of the wind model, since a steeper decline is expected for a jet geometry. Our failure to distinguish between different models of the circumburst medium can be attributed to the absence of radio measurements (particularly at millimeter wavelengths) at early times. The rapid rise of the flux density below ν_a and ν_m in the wind model and the strong frequency dependence of the peak flux (see Fig. 1) make such measurements advantageous (Panaitescu & Kumar 2000). Moreover, in principle, the wind model can be distinguished from the other models by the fact that in this model ν_c is increasing with time ($\nu_c \propto t^{1/2}$). However, in this case, since ν_c lies below the optical/IR bands, this behavior would be distinguishable only at late times when the host flux dominates over the optical transient. As before, we solved for the host flux and any dust extinction (see Table 3).

In summary, we find that the radio and optical/NIR observations of the afterglow emission from GRB 000418 can be fitted by two different models. The close similarity between the results of the wind and jet models has been noted for other GRBs: GRB 970508 (Frail et al. 2000; Chevalier & Li 2000), GRB 980519 (Frail et al. 2000b; Chevalier & Li 1999; Jaunsen et al. 2001), GRB 000301C (Berger et al. 2000; Li & Chevalier 2001), and GRB 991208 (Galama et al. 2000; Li & Chevalier 2001). The resolution of this conflict is important, since it goes to the core of the GRB progenitor issue. If the GRB progenitor is a massive star, then there must be evidence for a density gradient in the afterglow light curves, reflecting the stellar mass loss that occurs throughout the star's lifetime (Chevalier & Li 1999; Panaitescu & Kumar 2000). At present, an unambiguous case for a GRB afterglow expanding into a wind has yet to be found. On the contrary, most afterglows are better fitted by a jet expanding in a constant-density medium (e.g., Harrison et al. 1999; Halpern et al. 2000; Panaitescu & Kumar 2001), and thus we are faced with a peculiar situation. While there is good evidence linking GRBs to the dusty, gas-rich environments favored by hypernova progenitors (Bloom, Kulkarni, & Djorgovski 2000; Galama & Wijers 2001), the expected mass loss signature is absent (or at best ambiguous) in all afterglows studied to date.

A. D. is supported by a Millikan Fellowship at Caltech. GRB research at Caltech is supported by National Science Foundation and NASA grants (S. R. K.). K. H. is grateful for *Ulysses* support under JPL contract 958056 and for *NEAR* support under NAG 5-9503.

REFERENCES

Berger, E., et al. 2000, ApJ, 545, 56
Bessell, M. S., & Brett, J. M. 1988, PASP, 100, 1134
Bloom, J. S., Diercks, A., Djorgovski, S. G., Kaplan, D., & Kulkarni, S. R. 2000, GCN Circ. 661 (http://gcn.gsfc.nasa.gov/gcn3/661.gcn3)
Bloom, J. S., et al. 1998, ApJ, 508, L21
Bloom, J. S., Kulkarni, S. R., & Djorgovski, S. G. 2000, AJ, submitted (astro-ph/0010176)
Bloom, J. S., et al. 1999, Nature, 401, 453
Chevalier, R. A., & Li, Z.-Y. 2000, ApJ, 536, 195
———. 1999, ApJ, 520, L29
Frail, D. A., et al. 2000a, ApJ, 538, L129
———. 2000b, ApJ, 534, 559
Frail, D. A., Waxman, E., & Kulkarni, S. R. 2000, ApJ, 537, 191
Fukugita, M., Shimasaku, K., & Ichikawa, T. 1995, PASP, 107, 945
Galama, T. J., et al. 2000, ApJ, 541, L45
———. 1998, Nature, 395, 670
Galama, T. J., & Wijers, R. A. M. J. 2001, ApJ, 549, L209
Goodman, J. 1997, NewA, 2, 449
Granot, J., Piran, T., & Sari, R. 1999a, ApJ, 513, 679
———. 1999b, ApJ, 527, 236
Halpern, J. P., et al. 2000, ApJ, 543, 697
Harrison, F. A., et al. 1999, ApJ, 523, L121
Henden, A. 2000, GCN Circ. 662 (http://gcn.gsfc.nasa.gov/gcn3/662.gcn3)
Henden, A., et al. 2000, GCN Circ. 652 (http://gcn.gsfc.nasa.gov/gcn3/652.gcn3)
Hurley, K., Cline, T., & Mazets, E. 2000, GCN Circ. 642 (http://gcn.gsfc.nasa.gov/gcn3/642.gcn3)
Jaunsen, A. O., et al. 2001, ApJ, 546, 127
Jørgensen, I. 1994, PASP, 106, 967
Klose, S., et al. 2000a, ApJ, 545, 271
———. 2000b, GCN Circ. 645 (http://gcn.gsfc.nasa.gov/gcn3/645.gcn3)
Li, Z.-Y., & Chevalier, R. A. 1999, ApJ, 526, 716
———. 2001, ApJ, 551, 940
Livio, M., & Waxman, E. 2000, ApJ, 538, 187
Mészáros, P., & Rees, M. J. 1997, ApJ, 476, 232
Metzger, M. R., & Fruchter, A. 2000, GCN Circ. 669 (http://gcn.gsfc.nasa.gov/gcn3/669.gcn3)
Mirabal, N., Halpern, J. P., Kemp, J., & Helfand, D. J. 2000, GCN Circ. 646 (http://gcn.gsfc.nasa.gov/gcn3/646.gcn3)
Panaitescu, A., & Kumar, P. 2000, ApJ, 543, 66
———. 2001, ApJ, 554, 667
Piro, L., et al. 2000, Science, 290, 955
Reichart, D. E. 1999, ApJ, 521, L111
Rhoads, J. E. 1997, ApJ, 487, L1
———. 1999, ApJ, 525, 737
Sari, R., Piran, T., & Halpern, J. P. 1999, ApJ, 519, L17
Sari, R., Piran, T., & Narayan, R. 1998, ApJ, 497, L17
Schechter, P. L., Mateo, M., & Saha, A. 1993, PASP, 105, 1342
Schlegel, D. J., Finkbeiner, D. P., & Davis, M. 1998, ApJ, 500, 525
Taylor, J. H., & Cordes, J. M. 1993, ApJ, 411, 674
Tody, D. 1993, in ASP Conf. Ser. 52, Astronomical Data Analysis Software and Systems II, ed. R. J. Hanisch, R. J. V. Brissenden, & J. Barnes (San Francisco: ASP), 173
Wade, R. A., Hoessel, J. G., Elias, J. H., & Huchra, J. P. 1979, PASP, 91, 35
Walker, M. A. 1998, MNRAS, 294, 307 (erratum 321, 176 [2001])
Waxman, E. 1997, ApJ, 489, L33
Waxman, E., Kulkarni, S. R., & Frail, D. A. 1998, ApJ, 497, 288
Wijers, R. A. M. J., & Galama, T. J. 1999, ApJ, 523, 177

Note added in proof.—A. Fruchter & M. R. Metzger (Gen. Circ. 1061, http://gcn.gsfc.nasa.gov/gcn3/1061.gcn3 [2001]) have recently obtained *HST* observations, allowing them to subtract off the host galaxy contribution to the optical measurements. They find evidence for a steepening in the decay of the afterglow light curve at late times, in accordance with our findings based primarily on radio data.